Density Functional Theory Studies of the $Co(Cp)_2|V(CO)_6$ Radical-Pair System

Gerald M. Sando and Kenneth G. Spears*

Northwestern University, Department of Chemistry, 2145 Sheridan Road, Evanston, Illinois 60208-3113

Received: August 11, 2003; In Final Form: December 12, 2003

We have performed density-functional theory calculations for the $V(CO)_6$ radical, the $Co(Cp)_2$ radical, and the $Co(Cp)_2|V(CO)_6$ radical pair. Primary interest was in the $V(CO)_6$ radical in both the isolated species and in the radical pair. Several stable structures were found for the Jahn−Teller-active 17-electron $V(CO)_6$ radical for both the isolated radical and in the radical pair. We confirmed prior studies that identified a D_{3d} structure as most stable, a D_{4h} structure at higher energies, and a transition state of D_{2h} structure. We also found a new stable structure of C_{2h} geometry that is close ($\sim$130 cm^{-1}) to the lowest-energy D_{3d} structure. We calculated the relative energies of the isolated radical structures and the radical-pair structures as a function of the metal−metal distance. In addition, we estimated interconversion barriers between these structures and found similar results for both the isolated radical and the radical pair. This similarity suggests that the radical pair is rapidly interconverting at room temperature in the same manner as the isolated radical. This has implications in the interpretations of ultrafast electron-transfer dynamics. Specifically, a rise was observed for the radical carbonyl stretch vibration in the radical pair when the ion-pair charge-transfer absorption created excess vibrational energy in the radical pair. The rise time is not likely to be due to rapid geometric interconversion but is probably due to anharmonic coupling between highly excited low-frequency modes and the high-frequency carbonyl stretches leading to a broadened carbonyl absorption band immediately after excitation. The observed rise time in absorption is conjectured to correlate with cooling of the low-frequency vibrations to the solvent over 200 fs.

Introduction

The $[V(CO)_6^-|Co(Cp)_2^+]$ ion pair (Cp = cyclopentadiene) system shows interesting electron transfer (ET) dynamics. In solvents of low polarity, a contact ion pair is formed. The contact ion pair displays a broad ($\sim$7000 cm^{-1} full width at half maximum (fwhm)) and weak ($\epsilon \sim 125$ M^{-1} cm^{-1}) charge-transfer band in the visible, centered at 620 nm in CH_2Cl_2.[1] The photoinduced ET forms a radical pair that then undergoes rapid back ET to reform the ion pair. The vibrational relaxation (VR) of the carbonyl stretches is slower than the rate of back ET. This fact combined with the anharmonicity of the carbonyl stretches allows examination of the dependence of the ET rate on vibrational level.[2−4] Experiments on the picosecond time scale showed that the ET rate depended greatly on quantum number for the IR-active mode.[2,3] This was surprising since standard ET theories predict no effect due to population in IR-active modes whereas the important modes for ET rate control are the Raman-active modes. This suggested that the variation of the ET rate was due to a breakdown in the Condon approximation leading to a variation in the electronic coupling as a function of quantum number.

These facts motivated a re-examination of the ET dynamics on a faster time scale to examine the ultrafast dynamics of the system.[4] Following the Condon principle, the initial excitation should only populate the totally symmetric Raman-active modes. However, excited population is seen in the IR-active CO stretch, necessitating an intramolecular vibrational redistribution (IVR) process from the higher-frequency totally symmetric mode. Since no signs of IVR were seen in the picosecond experiments, femtosecond experiments were performed in hopes of observing the IVR process along with any ultrafast ET that may occur.

The ultrafast experiments revealed interesting behavior not only in the IVR process but also in the overall ET kinetics. In the femtosecond experiments, two ET components were seen, one around 700 fs and one about 5 ps. Only the ultrafast component showed a quantum level effect, but it was smaller than inferred with the picosecond data. The apparent rate variations in the picosecond experiments are attributed to a difference in relative contribution of the two ET components as a function of quantum level as is seen in the femtosecond experiments. The two ET components were assigned to two different ion-pair orientations in solution. In addition, interesting behavior was seen in rise times as a function of pump color due to VR and IVR processes. For pump colors on the low-energy side of the absorption band, a 200-fs rise time was resolved for $\nu = 2$ but no rise time was seen for $\nu = 1$ or $\nu = 0$. This is consistent with a two-quantum IVR conversion time of 200 fs and a one-quantum IVR time of <75 fs, the time resolution of the experiment. However, for pump colors at the peak and high-energy side of the absorption band, a 200-fs rise time was seen for all quantum levels. The origin of this rise time is not obvious because a rise time is not expected for the $\nu = 0$.

This rise time was tentatively assigned to a Jahn−Teller instability in the $V(CO)_6$ radical that results in a poorly defined infrared absorption band until the low-frequency modes are able to relax. The 17-electron radical species is expected to undergo a Jahn−Teller distortion from octahedral symmetry. This opens up the possibility of several different stable structures that can undergo interconversion. Interconversion can occur between two different forms of the same structure (differently oriented D_{3d}

* Author to whom correspondence may be addressed. E-mail: spears@chem.northwestern.edu. Fax: (847) 491-7713.

10.1021/jp036383f CCC: $27.50
Published on Web 01/21/2004

structures) or between two entirely different structures. Previous theoretical calculations in this lab have supported this idea with the lowest-energy structure having D_{3d} symmetry and a D_{2h} structure, lying ~200 cm^{-1} above the D_{3d} structure, with one imaginary frequency.[5,6] It was proposed that excess energy in low-frequency vibrations should allow fast interconversion between these and any other stable geometries, which could explain the lifetime broadening of the infrared band.[4] As the low-frequency vibrations relaxed, a well-defined frequency would appear, leading to a rise time in the IR absorption that corresponds to the VR process in the low-frequency modes. A related phenomenon of IR coalescence has been observed in organometallic systems that exhibit either rapid interconversion between two or more structures, either through intramolecular ET[7−11] or rapid rotation of a portion of the molecule.[12,13] The D_{2h} structure has been confirmed by other workers and reported to be a transition state between different forms of the more stable D_{3d} structure.[14]

Another possible source of spectral broadening is through anharmonic coupling between a low- and high-frequency mode. This is often referred to as the exchange mechanism,[15−18] where the high-frequency mode is anharmonically coupled to a low-frequency mode that exchanges energy with the bath. As opposed to a structural interconversion mechanism, this broadening mechanism can occur for a single geometry or be present simultaneous with geometric interconversion,[19−25] where the geometries need not have different frequencies.

If one treats the IR broadening in an analogous way to dynamic NMR, a site interchange model requires a change in frequency between sites to induce broadening followed by coalescence and narrowing as the exchange rate increases. However, there is a fundamental difference between IR and NMR due to the time scales of the processes involved. One assumption is that the transit time across the barrier is much less than the inverse of the difference in frequencies, a difficult requirement to satisfy in the infrared for some processes.[26] Even so, IR coalescence has been modeled with modified Bloch equations successfully,[7−13] although validity of this approach has been questioned.[27] However, the exchange mechanism results in a similar IR broadening and coalescence even without any exchange between sites.

The primary purpose of this manuscript is to explore the stability of various radical-pair structures. A secondary goal is to then use these results to examine the prior experimental interpretation. To accomplish this, the isolated radicals are first studied to provide a starting point for the radical-pair calculations, and the isolated radical structures are then placed together to form the pair. The resulting stable structures of the radical pair are then compared to those of the isolated radical for both relative energies and structural parameters of the $V(CO)_6$ moiety to test how the $Co(Cp)_2$ radical perturbs the $V(CO)_6$ structure. In addition, barriers to structural interconversion are estimated for both the isolated radical and the radical pair. The study of barriers is done to assess the likelihood of the proposed mechanism of the experimentally observed infrared rise times. Specifically, is excess energy in low-frequency modes likely to cause a rapid geometric interconversion leading to broadened infrared bands or must some other process, such as the anharmonic exchange model, be involved?

Theoretical Methods

All calculations were performed using Q-Chem 2.0.2.[28] Density-functional theory (DFT) was used, with both the B3LYP and BP86 functionals. Basis sets for the transition metals were identical to those used in Gaussian 98 and follow their naming conventions.[29] Basis sets for the remaining atoms were built into Q-Chem and are named as in the Gaussian convention. Geometry optimizations of the isolated radicals were performed with full symmetry constraints except for the cases with D_{3d} symmetry, which were performed in the C_{2h} subgroup. Optimizations were repeated with slightly distorted C_1 symmetry structures and resulted in no change except a larger than expected difference in energy when full D_{3d} symmetry was used rather than the C_{2h} subgroup. The radical pair was calculated as a triplet state to prevent convergence on an ion-pair electronic structure. Optimizations of the entire radical pair were performed with the coordinates of the $Co(Cp)_2$ radical frozen at the staggered C_{2h} structure of the isolated radical. The position of the vanadium atom was also fixed, leading to a fixed Co−V distance. Optimizations were repeated for several Co−V distances. The energies of the optimized structures were used to construct a potential as a function of the Co−V distance.

Barriers to interconverting various structures in both the isolated radical and the radical pair were performed in two steps. First, a reaction coordinate was chosen along the Cartesian vector of the difference between the two structures. Single-point calculations were done on 10 equally spaced points along this reaction coordinate. This provided an initial upper bound estimate of the barrier. If a barrier was initially seen, a better estimate of the barrier was found by performing additional geometry optimizations for the initial points on the reaction coordinate with the addition of constraints on the coordinates of two adjacent carbon atoms, leading to a reaction coordinate primarily determined by the CVC angle. Attempts to freeze only the CVC angle rather than the carbon coordinates failed. For the radical pair, the coordinates of the two carbons facing the $Co(Cp)_2$ were fixed. For the isolated $V(CO)_6$ radical, adjacent carbons with the proper CVC angle were frozen to be analogous to the radical pair. This procedure resulted in a smaller calculated barrier and provided a better upper bound estimate of the true barrier.

Results

$V(CO)_6$ Radical. Four stable structures were found for the $V(CO)_6$ radical species for all basis sets with both the B3LYP and BP86 functionals, with two exceptions. The symmetries of the structures in increasing energetic order are D_{3d}, C_{2h}, D_{2h}, and D_{4h}. The C_{2h} structure is a previously unreported structure, but the other structures have been previously reported by us (D_{3d}, D_{2h})[5,6] and others (D_{3d}, D_{2h}, D_{4h}).[14] The relative energies as a function of method and basis set are given in Table 1. The energies are relatively independent of basis set with the D_{3d} structure always the lowest-energy structure; however, the two functionals have small differences. By use of the energy of the D_{3d} structure as the zero of energy, the B3LYP and BP86 functionals result in a C_{2h} structure with a similar relative energy of ~130 cm^{-1}, with the exact value depending on the basis set. The relative energy of the D_{2h} structure is calculated to be approximately 250 cm^{-1} for B3LYP and 360 cm^{-1} for BP86. The highest-energy structure studied, the D_{4h} structure, has a relative energy of 570 cm^{-1} for B3LYP and 780 cm^{-1} for BP86. The two exceptions referred to previously are for the two largest basis sets using the B3LYP method where our attempts at finding a D_{4h} structure failed.

Table 2 shows the structural parameters for the 6-311G* basis set, the largest basis set where all structures were found for both DFT methods. The distortion from octahedral symmetry of the D_{3d} structure is a tetragonal distortion of the CVC angles

TABLE 1: Relative Energies of the Various Structures of the $V(CO)_6$ Radical (in cm^{-1}) as a Function of Basis Set and DFT Method[a]

	D_{3d}	C_{2h}	D_{2h}	D_{4h}
	B3LYP			
6-311G/6-31G*	0	104	253	568
6-311G/6-311G*	0	130	273	573
6-311G*	0	123	268	570
6-311+G/6-311G(2d)	0	86	194	
6-311+G(2d)	0	101	244	
	BP86			
6-311G/6-31G*	0	116	343	769
6-311G/6-311G*	0	121	350	765
6-311G*	0	121	360	773
6-311+G/6-311G(2d)	0	141	387	834
6-311+G(2d)	0	150	377	774

[a] The basis set is given as (V)/(C,O) if a different basis set was used for the V atom.

TABLE 2: Bond Lengths and Angles for the Various Structures of the $V(CO)_6$ Radical[a]

	VC (Å)	CO (Å)	CVC	VCO
		B3LYP/6-311G*		
D_{3d}	2.017 (6)	1.141	93.8°, 86.2° (6)	179.2° (6)
C_{2h}	2.027 (2)	1.140 (2)	94.7°, 85.3° (2)	178.6° (2)
	2.013 (4)	1.141 (4)	91.1°, 88.9° (4)	178.7° (4)
D_{2h}	2.038 (2)	1.139 (2)	95.1°, 84.9° (2)	180° (2)
	2.008 (4)	1.142 (4)	90° (8)	179.3° (4)
D_{4h}	1.983 (2)	1.145 (2)	90° (12)	180° (6)
	2.036 (4)	1.139 (4)		
		BP86/6-311G*		
D_{3d}	1.999 (6)	1.155 (6)	94.1°, 85.9° (6)	179.5° (6)
C_{2h}	2.005 (2)	1.155 (2)	94.8°, 85.2° (2)	178.4° (2)
	1.995 (4)	1.156 (4)	92.1°, 87.9° (4)	178.6 (4)
D_{2h}	2.018 (2)	1.153 (2)	95.5°, 84.8° (2)	180° (2)
	1.992 (4)	1.157 (4)	90° (8)	179.4° (4)
D_{4h}	1.970 (2)	1.159 (2)	90° (12)	180° (6)
	2.014 (4)	1.153 (4)		

[a] Numbers in parentheses indicate the number of bond lengths or angles with the given value. Opposite pairs of carbonyl groups are equivalent in all structures.

by approximately 4° with a nearly linear (within 1°) VCO angle for both computational methods. The VC and CO bond lengths are 2.017 and 1.141 Å for B3LYP and 1.999 and 1.155 Å for BP86. The distortion from octahedral symmetry of the C_{2h} structure is similar to the D_{3d} structure with one opposing pair of CO groups undergoing a different distortion in bond length and angles than the others. One pair of CO groups is distorted from 90° by about 5°, with the other 4 carbonyls distorting by a lesser amount of about 2° for both methods. The VCO angles are distorted from linearity by about 1.5°. Again the bond lengths show a dependence on DFT method with B3LYP favoring longer VC bonds and shorter CO bonds for all structures. The two unique carbonyl groups have longer (~0.01 Å) VC bonds and slightly shorter (~0.001 Å) CO bonds than the other four. The D_{2h} structure has one pair of carbonyls distorted from 90° by about 5°, like the C_{2h} structure, but the remaining CVC angles are 90°. Two of the VCO angles are linear as required by symmetry with the other four within 1° of linearity. The two unique carbonyls groups have longer (0.03 Å for B3LYP, 0.026 Å for BP86) VC bonds and somewhat shorter (0.003 Å for B3LYP, 0.004 Å for BP86) CO bonds than the other four. The D_{4h} structure has all 90° CVC and linear VCO angles as is required by symmetry. However, there are again two unique carbonyls with shorter (0.053 Å for B3LYP, 0.044 Å for BP86) VC bonds and somewhat longer (0.006 Å) CO bonds than the remaining CO groups.

TABLE 3: Calculated IR-Active CO Stretches (in cm^{-1}) of Isolated $V(CO)_6$ for Both Methods and Two Different Basis Sets

D_{3d}	C_{2h}	D_{2h}	D_{4h}[a]
	B3LYP/6-311G(V), 6-31G*(C,O)		
2075*	2073	2069	2055
2078	2075	2072	2088*
	2082	2091	
	BP86/6-311G(V), 6-31G*(C,O)		
1987*	1972	1981	1975
1989	1973	1983	1994*
	1985	2000	
	B3LYP/6-311G*		
2068*	2065	2061	2043
2071	2067	2064	2081*
	2076	2084	
	BP86/6-311G*		
1978*	1977	1972	1964
1980	1978	1974	1989*
	1984	1992	

[a] An asterisk indicates a 2-fold degenerate mode.

Vibrational frequency calculations were performed for the four structures, and the results for the IR active carbonyl modes are given in Table 3. Results for both the 6-311G* basis set and the basis set used for the radical-pair calculations, 6-311G on vanadium and 6-31G* on carbon and oxygen, are shown. The most important feature is the similarity between frequencies of the IR-active modes, especially the three lowest-energy structures. The experimental IR line width for the ion pair system of experimental interest is about 40 cm^{-1} fwhm in CH_2Cl_2; however, this was assigned to have contributions from two ion-pair geometries.[4] In the radical pair, a similar line width would be expected only if the excitation wavelength would populate both geometries. Even a line width of 20 cm^{-1} would lead to experimentally unresolved IR bands for the various $V(CO)_6$ structures since the shifts are not large. It should be noted that the frequency calculation for the D_{2h} structure identifies it as a transition state with one imaginary vibrational frequency, and this result is independent of basis set and method.

In summary, the results of the DFT calculations have minor differences that are due to method and basis set, and the differences are mainly in the bond lengths and vibrational frequencies between B3LYP and BP86. However, within one method, the relative changes for different geometries are similar.

$Co(Cp)_2$ Radical. Calculations on the other half of the radical pair, the $Co(Cp)_2$ radical where Cp = cyclopentadiene, were performed for a much more limited range of basis sets. This radical is also expected to distort from ideal symmetry due to Jahn−Teller effects. As expected, the Cp rings are found to break their 5-fold symmetry to give Cp rings with approximately C_{2v} symmetry. Several stable structures of the $Co(Cp)_2$ radical were found including eclipsed, staggered, and slightly twisted from both the staggered and eclipsed forms. All were close in energy and were found to have one imaginary vibrational frequency, both most likely due to the ease of relative rotation of the Cp rings. Attempts to find a true minimum by breaking symmetry between the Cp rings failed, resulting in structures with identical Cp rings equidistant from the cobalt. This suggests that the Cp rings are equivalent and free to rotate, especially in condensed phases at room temperature. These results are consistent with previous DFT calculations, indicating small energy differences between structures and a reduction in symmetry due to Jahn Teller effects.[30,31] The staggered C_{2h} form was used in the radical-pair calculations.

TABLE 4: Comparison of Bond Lengths and Angles for $V(CO)_6$ as Isolated $V(CO)_6$ Radical and in the $Co(Cp)_2|V(CO)_6$ Radical Pair[a]

	B3LYP/6-311G(V, Co), 6-31G**(C,O,H)				
	isolated D_{3d}	D_{3d} wide	D_{3d} narrow	isolated D_{2h}	D_{2h} narrow
VC (Å)	2.013 (6)	2.007 (2)*	2.008/2.010 (2)*	2.002 (4)	1.999 (2)*
		2.012 (2)	2.011/2.012 (2)		2.002 (2)
		2.012/2.015 (2)	2.009/2.012 (2)	2.030 (2)	2.033/2.031 (2)
CO (Å)	1.15 (6)	1.151 (2)*	1.151 (2)*	1.151 (4)	1.152 (2)*
		1.150 (2)	1.150 (2)		1.151 (2)
		1.150/1.149 (2)	1.150 (2)	1.148 (2)	1.147 (2)
CVC	93.7°/86.3° (6)	96.5°*	~90°*	85.0° (2)	88.3°*
		92.9°	85.5°		84.2°

[a] Numbers in parentheses indicate the number of bond lengths or angles with the given value. Numbers marked with an asterisk correspond to bonds or bond angles closest to the $Co(Cp)_2$ group. The radical-pair structures are for a metal−metal separation of 5.7 Å. The bottom row for each set of bond lengths corresponds to bonds approximately perpendicular to the V−Co axis and the planes of the Cp rings. For the CVC angles, only the angle adjacent to and opposite of the $Co(Cp)_2$ group is included.

$Co(Cp)_2|VCO_6$ Radical Pair. Because of the size of the radical-pair system, the basis set was limited to 6-311G on V and Co and 6-31G** on the remaining atoms. In addition, all attempts using BP86 failed to converge so calculations were limited to the B3LYP method. The radicals were aligned so that the vanadium was positioned on the mirror plane of the $Co(Cp)_2$ that contains the cobalt atom and bisects the staggered Cp rings. Four CO groups were aligned approximately in a plane that is perpendicular to the $Co(Cp)_2$ mirror plane, contains the vanadium and cobalt atoms, and is parallel to the Cp rings. The Co−V line bisects two pairs of CO groups. This left two remaining carbonyl groups that were approximately parallel to the $Co(Cp)_2$ mirror plane. If the vanadium moiety had two unique carbonyls groups, they were placed in this location approximately parallel to the $Co(Cp)_2$ mirror plane. The vanadium position was fixed, and the initial positions of other atoms were from optimized structures, but some ambiguity remains in how to arrange the various structures to form the initial structure of the radical pairs. There are two choices for the angle between the carbons in the carbonyl groups that point toward the $Co(Cp)_2$ radical, either greater than or less than 90°. Both of these possibilities were studied with the greater than 90° case referred to as wide angle and the less than 90° referred to as narrow angle. For the D_{3d} and C_{2h} $V(CO)_6$ structures before and after optimization, the wide-angle forms had overall C_s symmetry and the narrow angle forms had C_1 symmetry. Both forms had C_s symmetry for the D_{2h} structure and only one structure of C_s symmetry resulted for the D_{4h} structure with all 90° CVC angles.

Geometry optimizations were performed with the $Co(Cp)_2$ and vanadium coordinates frozen for a range of V−Co distances. The wide- and narrow-angle forms using the D_{3d} $V(CO)_6$ structure resulted in a radical pair that had $V(CO)_6$ units with structures very similar to the D_{3d} structure of the isolated radical. However, there was some distortion from the D_{3d} structure, especially for the carbonyl groups closest to the $Co(Cp)_2$. These two radical-pair structures are referred to as D_{3d} wide and D_{3d} narrow. Radical-pair optimizations that were performed starting with the C_{2h} $V(CO)_6$ structure resulted in structures that were nearly identical to those found with the D_{3d} structure so this starting configuration gave no new results. Radical-pair optimizations that were performed starting with both the wide angle and narrow angle form of the D_{2h} $V(CO)_6$ structure resulted in the same final structure, which had approximate D_{2h} symmetry for the $V(CO)_6$ and a narrow-angle-type structure. This is referred to as D_{2h} narrow. It is unclear as to why no wide-angle structure was found to be stable. Radical-pair structures using the D_{4h} $V(CO)_6$ structure were initially pursued, and stable structures with approximate D_{4h} symmetry for the $V(CO)_6$ moiety were found for several V−Co distances; however, this avenue was abandoned due to the higher energy expected of this structure. We compare some of the key bond lengths and angles for isolated $V(CO)_6$ and radical pairs containing $V(CO)_6$ in Table 4. We note that the angle changes for each radical-pair geometry are the major changes, while the bond lengths are only slightly different.

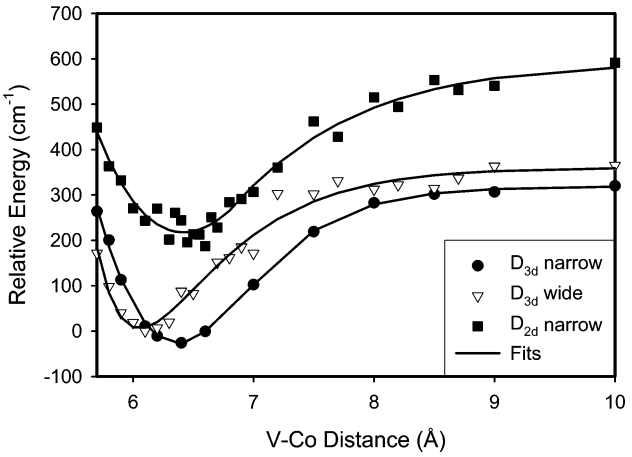

Figure 1. Calculated energies of $Co(Cp)_2|V(CO)_6$ D_{3d} wide (▽), D_{3d} narrow (●), and D_{2h} narrow (■) radical-pair structures for a range of metal separation distances. Included are fits to a Morse potential for the D_{3d} wide structure and two Morse potentials for the narrow angle structures.

The relative energies of the three radical-pair structures are plotted as a function of the V−Co distance in Figure 1. Shown along with the points is a fit to a single Morse potential for the D_{3d} wide and a fit to two Morse potentials, each for a different range of distances, for the two narrow structures. The narrow-angle structures did not fit well to a single Morse potential near the bottom of the potential, most likely due to the ability of the CVC angle to distort without a large energetic penalty to offset the steric interaction for the smaller V−Co distances. No physical meaning is attributed to the double Morse potential fit. The fit only serves as an empirical fitting function. Not surprisingly, the minima differ for the wide vs the narrow angle structures due to steric effects. The D_{3d} wide minimum is at 6.1 Å, while the minima for the D_{3d} narrow and D_{2h} narrow are slightly longer at 6.4 Å. As is expected from the isolated radical calculations, the D_{2h} form is higher in energy than either D_{3d} form. In addition, the D_{3d} wide form is favored at very short distances, as would be expected due to steric effects. However, the D_{3d} narrow form is more stable over most of the range studied. The calculated structures reveal that the $V(CO)_6$ portion of radical pairs are practically identical in structure to the isolated

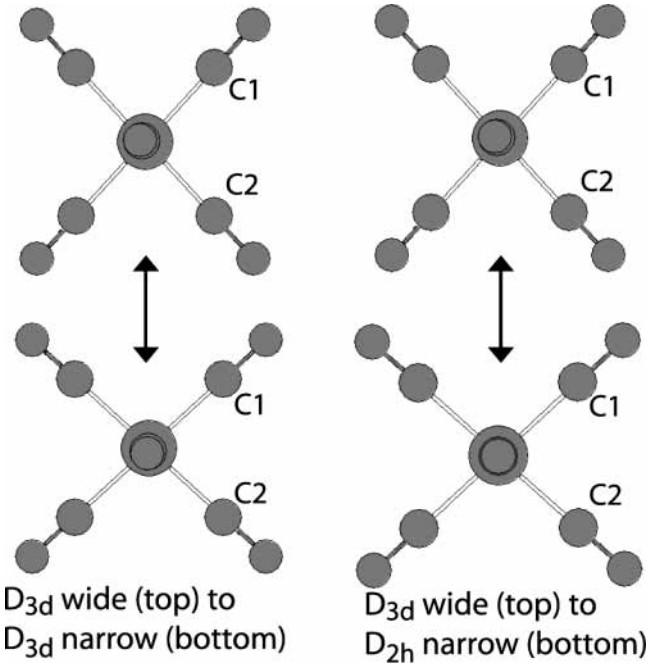

Figure 2. Initial and final structures used in estimations of interconversion barriers. Coordinates of C1, C2, and the vanadium are fixed along the reaction path while the remaining atoms are allowed to optimize. The angle between C1, V, and C2 is described as wide or narrow where narrow is 86.3° (D_{3d}) or 84.0° (D_{2h}) and wide is 93.7° (D_{3d}).

radical at the longer Co−V distances studied. As the Co−V distance is shortened, the $V(CO)_6$ portion undergoes a distortion that primarily shortens the VC bond length and widens the CVC angle for the two carbonyl groups facing the $Co(Cp)_2$ fragment as would be expected due to steric effects. The decrease in the VC bond lengths also creates a secondary effect of increasing the two VC bond lengths for the carbonyls perpendicular to the V−Co axis.

VCO_6 Radical Interconversion Barriers. Barriers to interconversion between different structures were estimated for the isolated $V(CO)_6$ radical species. For structures where no CVC angle crosses 90°, no barrier was seen; instead, monotonic increase or decrease in energy was seen as the geometry was scanned from one structure to another. This included the interconversion between the D_{3d} and D_{2h} structures oriented so that the structures are most similar. This corresponds to the $V(CO)_6$ moiety in the D_{3d} narrow and D_{2h} narrow radical-pair structures. However, to calculate interconversion barriers for the isolated radical that correspond to converting from a wide- to a narrow-angle radical-pair structure, the initial and final isolated radical structures must be oriented so that the geometric change corresponds to what is seen in the radical-pair structures. The two barriers of interest are converting between two D_{3d} structures, that are rotated by 90° relative to each other, and between the D_{3d} and D_{2h} structures where there is an interchange of acute and obtuse angles. These structures are shown in Figure 2. These correspond to the radical pair converting from the wide D_{3d} structure to either the narrow D_{3d} structure or the narrow D_{2h} structure, respectively. Wide and narrow refer to the angle that is formed by the metal and two carbons that are fixed in the optimization. In Figure 2, the fixed angle between C1, V, and C2 is described as wide or narrow where narrow is 86.3° (D_{3d}) or 84.0° (D_{2h}) and wide is 93.7° (D_{3d}). As expected, the initial geometry scans revealed a barrier for both processes. The next step of the barrier-estimating process, optimizing with the vanadium and two adjacent carbons in fixed positions, revealed

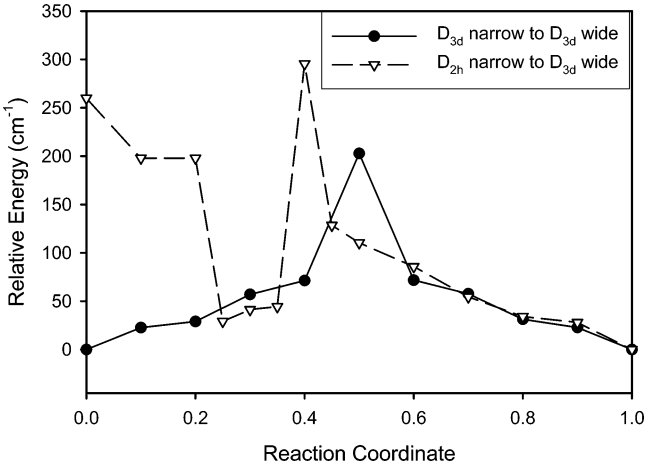

Figure 3. B3LYP/6-311G(V), 6-31G*(C,O) estimates of barriers to interconversion between radical geometries of isolated $V(CO)_6$. The reaction coordinate goes from either a D_{3d} narrow (●, solid line) or D_{2h} narrow (▽, dashed line) structure to a D_{3d} wide structure (value of 1). Energies were calculated by optimizing structure with the coordinates for vanadium and two carbon atoms fixed along the direct path connecting the structures. The dip in the D_{2h} narrow to D_{3d} wide is from a local geometry of C_{2h} symmetry.

a somewhat smaller barrier. The estimates of the barriers are approximately 200 cm^{-1} for the D_{3d} narrow to D_{3d} wide conversion and 350 cm^{-1} above the D_{3d} energy for the D_{2h} narrow to D_{3d} wide conversion. The energies as a function of reaction coordinate are shown in Figure 3. It should be mentioned that these are upper-bound values for the reaction barrier, the true value may be lower. The dip in the D_{2h} narrow to D_{3d} wide potential is due to a region that structurally resembles the C_{2h} structure. Additional points in this region were calculated to confirm the general shape of the potential.

Co(Cp)2|VCO6 Radical-Pair Interconversion Barriers. The barriers for interconversion between the various radical-pair structures were also estimated. The barriers were estimated at a fixed V−Co distance of 5.7 Å, the shortest V−Co distance studied, which favors the D_{3d} wide structure. This was done for two reasons; first, it is most appropriate for comparison to experiment where the radical pair is initially formed near the shorter ion pair separation distance and, second, to maximize the effect of the $Co(Cp)_2$ on the barrier height. For the D_{3d} narrow to D_{2h} narrow process, where no CVC angle crosses 90°, the initial scan revealed no barrier. This is similar to what was seen in the isolated radical. For the interconversion between the D_{3d} narrow and D_{3d} wide and between the D_{2h} narrow and D_{3d} wide structures, the initial scan revealed a significant barrier. The optimization fixed the coordinates of the carbons facing the cleft between the Cp planes in $Co(Cp)_2$ (see Figure 2, C1 and C2). A lower barrier height was found for the optimizations where for the D_{3d} narrow and D_{3d} wide process, the barrier is estimated to be 175 cm^{-1} above the D_{3d} wide energy. For the D_{2h} narrow and D_{3d} wide process the barrier is estimated to be 350 cm^{-1} above the D_{3d} wide energy. The energy as a function of reaction coordinate for both processes is given in Figure 4.

Discussion

$V(CO)_6$ Radical. The results for the isolated radical structures are consistent with previous studies.[5,6,14] A recent DFT study used the BP86 functional to study the $V(CO)_6$ radical and also reported experimental measurements.[14] In this study, the D_{3d} structure was found to be the most stable with a D_{2h} and a D_{4h} structure at higher energy. The relative energies of the structures

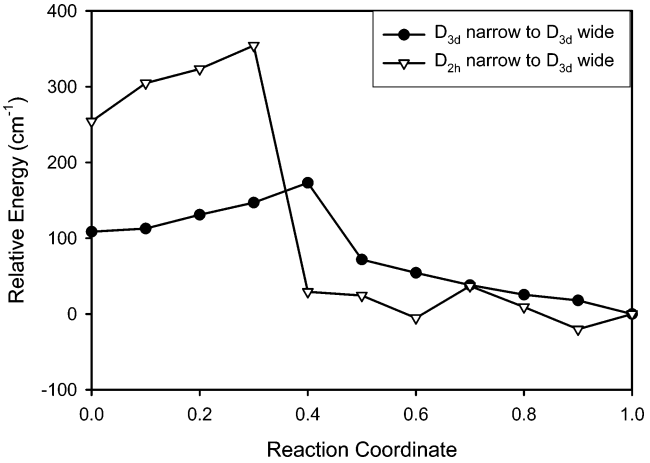

Figure 4. B3LYP/6-311G(V), 6-31G**(C,O,H) estimates of barriers to reaction for different structures of $V(CO)_6$ in the radical pair $Co(Cp)_2|V(CO)_6$. The reaction coordinate is for $V(CO)_6$, evolving from either the D_{3d} narrow (●, solid line) or D_{2h} narrow (▽, solid line) structure to the D_{3d} wide structure (value of 1). Energies were calculated by optimizing the $V(CO)_6$ structure with the coordinates for vanadium and the two carbon atoms closest to the $Co(Cp)_2$ fixed along the direct path connecting the structures.

are similar to what we find here with differences attributed to differing methods and basis sets. Also consistent with our previous results and recent work, the D_{2h} structure is found to have an imaginary frequency for all basis sets and methods,[14] indicating that this structure is not a stable minimum. However, we find a new stable low-energy structure that appears to be a true local minimum with all real vibrational frequencies for all basis sets and methods. This new structure is of lower symmetry (C_{2h}) than the previously known structures and is only slightly higher in energy than the most stable D_{3d} structure but lower in energy than the other previously reported structures.

Barriers to interconverting different structures were found to be either fairly small or nonexistent, depending on whether the CVC angle crosses 90°. This is consistent with the recent DFT study of the $V(CO)_6$ radical system.[14] This study included molecular dynamics (MD) simulations that suggested rapid interconversion at room temperature, resulting in an averaged structure that has approximately octahedral symmetry with very similar radial distributions as the octahedral $V(CO)_6^-$ species.[32,33] At low temperature, the dynamic Jahn−Teller distortions become a static distortion and the radical remains in the favored D_{3d} structure. This is reflected in a change in the radial distribution from the MD simulations. These results are consistent with experiments, where low-temperature EPR data is consistent only with the D_{3d} structure.[14] The vapor-phase electron diffraction, performed at 62 °C, suggests an octahedral structure with a dynamic Jahn−Teller effect[34] and gives a radial distribution that is in general agreement with the radial distributions from the MD simulations.[14]

$Co(Cp)_2|VCO_6$ Radical Pair. Not surprisingly, the relative energies of the various radical-pair structures depend on distance. At short V−Co distances, the D_{3d} wide is favored as would be expected due to steric effects, and at larger distances, the D_{3d} narrow is favored with the potentials crossing at a distance just above 6.1 Å. The D_{2h} narrow structure is higher in energy, with the energy difference also dependent upon the metal−metal distance. This is not surprising due to the differing nature of the narrow and wide structure potentials near their minima along with the differing location of the minima. Previous DFT calculations[6] have placed the ion-pair equilibrium separation in solution to be about 5.9 Å. The Condon principle predicts that the initially formed radical pair will be near the equilibrium structure of the ion pair, somewhere between 5.5 and 6.2 Å, the thermally accessible range of ion-pair distances. Over most of this range, the D_{3d} wide structure is favored energetically, although not by very much.

It was previously suggested that the origin of a 200-fs IR rise time seen in an ultrafast ET experiment was due to the existence of several interconverting Jahn−Teller structures broadening the IR band until the system vibrationally relaxed into a single structure.[4] Since it has been shown that the isolated radical does not remain in a single structure at room temperature,[14] the radical pair was compared to the isolated radical in terms of barriers to geometric interconversion. This was performed at the shortest V−Co distance studies, 5.7 Å, to maximize any perturbations due to the $Co(Cp)_2$ in addition to being in the range of expected V−Co distances in the initially formed species. Our estimates of barriers to geometric interconversion in the radical pair are very similar in magnitude to the isolated radical, even at the small separation distance of 5.7 Å. The radical pair is expected to be even more like the isolated radical at larger separation distances. Therefore we expect rapid geometric interconversion for the radical pair leading to averaged structures just like in the isolated radical even after vibrational relaxation has taken place. We have calculated vibrational frequencies only for isolated $V(CO)_6$, and because of the similar structure in the radical pair we expect little change in vibrations for $V(CO)_6$ in radical pairs. The radical-pair geometry is sufficiently large that vibrational calculations would take a long time.

Origin of the Experimental Rise Time. These theoretical results suggest that a different mechanism is responsible for the experimentally observed rise time. Even without the dynamic rather than static Jahn−Teller effect expected at room temperature, the very broad IR bands combined with the calculated frequencies for the different structures would not lead to highly broadened spectra below the detection limit, which was the conjectured source of a rise time. An exchange process analogous to dynamic NMR would not lead to sufficiently broadened spectra in this type of system, so another type of mechanism must be responsible for the observed rise time seen only for high-frequency pump colors.

Since it has been shown that the high-frequency pump colors must deposit more excess vibrational energy in low-frequency modes than lower-frequency pump colors,[4] these modes are still a likely cause of the rise time feature. One possible explanation is the fact that several low-frequency modes must be very anharmonic due to the many stable Jahn−Teller structures that are related by fairly small angle changes. This leads to the expectation of large anharmonic couplings between the low-frequency modes and the carbonyl stretches, especially since the carbonyl stretches are themselves anharmonic enough to see a shift in frequency for hot bands. One of the results of anharmonic couplings is that the carbonyl frequency should be dependent upon the number of quanta in these low-frequency modes.[20] The higher-frequency pump experiments should lead to a wide distribution of populations of various low-frequency modes. This wide population distribution along with the many low-frequency modes should lead to a much broader spectrum than is seen after relaxation. If the oscillator strength of the IR band is conserved, it is certainly in the realm of possibility that the carbonyl band is broadened enough to not be observable with the signal−noise of the experiment. As the low-frequency modes relax, leading to a narrower carbonyl band, the IR signal

will appear to grow in with a rise time similar to that of the low-frequency vibrational relaxation process.

Similar broadening mechanisms have been used to describe the width of vibrational bands in condensed-phase polyatomic molecules.[15−18] In addition, a similar mechanism has been proposed for broadening of IR bands where there is a multiple well potential along a low-frequency mode where exchange between wells does not properly account for the line width,[19−25] a similar situation to the radical pair. The lack of a large carbonyl frequency change as a function of geometry rules out a simple site-exchange mechanism for the broadening. In addition to the energy minima, frequency calculations were performed for structures corresponding to the top of the radical interconversion barriers for the isolated $V(CO)_6$. These resulted in carbonyl frequencies that were identical to the frequencies for the minima within the experimental line width. This points to a difference between the current study and the previous studies of the anharmonic mechanism. The previous studies dealt with a classical low-frequency coordinate with a high-frequency mode that changed frequency along the potential surface formed by the low-frequency mode. The current study deals with highly excited quantum vibrations where the anharmonic frequency shifts should be larger than for thermally relaxed species. In this case, the vibrational relaxation is like the exchange process with the bath, except that it is irreversible since the radical pair is initially in a nonequilibrium state undergoing relaxation rather than at equilibrium as is assumed in the previous studies. This initial population distribution is similar to a high-temperature distribution, with the addition of irreversibility. This should lead to greater spectral broadening than was seen for the equilibrium species for a given anharmonic coupling. This is consistent with the experiment where the IR band narrows and appears to grow in as equilibrium is reached. Although much of this discussion is admittedly speculative, it appears to provide a more likely alternative explanation for the origin of the experimental rise time. A true test of these ideas is beyond the scope of this work, and should prove to be very interesting and provide more insight into the vibrational relaxation process.

Conclusion

We have performed DFT calculations for the $V(CO)_6$ radical for a range of basis sets using the B3LYP and BP86 functionals. Several stable structures were found, including a previously unreported C_{2h} structure that is very close in energy (∼130 cm^{-1}) to the most stable D_{3d} structure. Barriers to interconversion were estimated and found to be small to nonexistent, depending on the nature of the geometric distortion that had to occur. This was consistent with previously reported MD simulation that suggested a dynamic rather than static Jahn−Teller effect in this molecule at room temperature, resulting in rapidly interchanging structures with an octahedral averaged structure.

B3LYP calculations on the related $Co(Cp)_2|V(CO)_6$ radical pair revealed a situation very similar to the isolated radical. Several stable Jahn−Teller structures were found. Barriers to interconversion were also found to be very similar to what was seen in the isolated radical. It appears that the $Co(Cp)_2$ radical only slightly perturbs the energetics of the $V(CO)_6$ radical. This leads to the conclusion that the radical pair must be experiencing a dynamic rather than static Jahn−Teller effect, with rapidly interchanging structures at room temperature. This has an impact on the interpretation of prior ultrafast ET experiments. In these experiments, visible photoexcitation of an ion pair creates a radical pair, and the back ET is followed by monitoring the carbonyl stretches in the infrared as a function of quantum number. A rise time of 200 fs was seen for the $\nu = 0$ level only for pump colors in the higher-energy portion of the charge-transfer band. This was tentatively interpreted as excess low-frequency vibrational population increasing the rate of geometric interconversion, leading to lifetime broadening of the IR band. However, the similarities between the vibrational frequencies of the isolated radical and the low barriers for dynamic interchange for the isolated radical and radical pair species show that this explanation is not sufficient. Instead, a mechanism involving anharmonic coupling between the initially highly excited low-frequency modes and the carbonyl stretches is a more likely candidate to explain the broadening and subsequent narrowing of the IR band with vibrational relaxation.

Acknowledgment. We thank the U.S. Department of Energy, Office of Science (Grant DE-FG02-91ER14228) for financial support.

References and Notes

(1) Bockman, T. M.; Kochi, J. K. *J. Am. Chem. Soc.* **1989**, *111*, 4669−4683.
(2) Spears, K. G.; Wen, X.; Arrivo, S. M. *J. Phys. Chem.* **1994**, *98*, 9693−9696.
(3) Spears, K. G.; Wen, X.; Zhang, R. *J. Phys. Chem.* **1996**, *100*, 10206−10209.
(4) Marin, T. W.; Homoelle, B. J.; Spears, K. G. *J. Phys. Chem. A* **2002**, *106*, 1152−1166.
(5) Sando, G. M.; Spears, K. S. *J. Phys. Chem. A* **2001**, *105*, 5326−5333.
(6) Spears, K. G.; Shang, H. *J. Phys. Chem. A* **2000**, *104*, 2668−2680.
(7) Yamaguchi, T.; Imai, N.; Ito, T.; Kubiak, C. P. *Bull. Chem. Soc. Jpn.* **2000**, *73*, 1205−1212.
(8) Londergan, C. H.; Salsman, J. C.; Ronco, S.; Dolkas, L. M.; Kubiak, C. P. *J. Am. Chem. Soc.* **2002**, *124*, 6236−6237.
(9) Ito, T.; Yamaguchi, T.; Kubiak, C. P. *Macromol. Symp.* **2000**, *156*, 269−275.
(10) Ito, T.; Hamaguchi, T.; Nagino, H.; Yamaguchi, T.; Kido, H.; Zavarine, I. S.; Richmond, T.; Washington, J.; Kubiak, C. P. *J. Am. Chem. Soc.* **1999**, *121*, 4625−4632.
(11) Ito, T.; Hamaguchi, T.; Nagino, H.; Yamaguchi, T.; Washington, J.; Kubiak, C. P. *Science* **1997**, *277*, 660−663.
(12) Turner, J. J.; Grevels, F.-W.; Howdle, S. M.; Jacke, J.; Haward, M. T.; Klotzbücher, W. E. *J. Am. Chem. Soc.* **1991**, *113*, 8347−8353.
(13) Turner, J. J.; Gordon, C. M.; Howdle, S. M. *J. Phys. Chem.* **1995**, *99*, 17532−17538.
(14) Bernhardt, E.; Willner, H.; Kornath, A.; Breidung, J.; Buhl, M.; Jonas, V.; Thiel, W. *J. Phys. Chem. A* **2003**, *107*, 859−868.
(15) Harris, C. B.; Shelby, R. M.; Cornelius, P. A. *Phys. Rev. Lett.* **1977**, *38*, 1415−1419.
(16) Shelby, R. M.; Harris, C. B.; Cornelius, P. A. *J. Chem. Phys.* **1979**, *70*, 37−41.
(17) Marks, S.; Cornelius, P. A.; Harris, C. B. *J. Chem. Phys.* **1980**, *73*, 3069−3081.
(18) Nitzan, A.; Persson, B. N. J. *J. Chem. Phys.* **1985**, *83*, 5610−5618.
(19) Wood, K. A.; Snyder, R. G.; Strauss, H. L. *J. Chem. Phys.* **1989**, *91*, 5255−5267.
(20) Wood, K. A.; Strauss, H. L. *J. Phys. Chem.* **1990**, *94*, 5677−5684.
(21) Lascombe, J.; Cavagnat, D.; Lassegues, J. C.; Rafilipomanana, C.; Biran, C. *J. Mol. Struct.* **1984**, *113*, 179−190.
(22) Corn, R. M.; Strauss, H. L. *J. Chem. Phys.* **1982**, *76*, 4834−4843.
(23) MacPhail, R. A.; Snyder, R. G.; Strauss, H. L. *J. Chem. Phys.* **1982**, *77*, 1118−1137.
(24) Cavagnat, D.; Lascombe, J. *J. Chem. Phys.* **1982**, *76*, 4336−4348.
(25) MacPhail, R. A.; Snyder, R. G. *J. Chem. Phys.* **1989**, *91*, 3895−3902.
(26) MacPhail, R. A.; Strauss, H. L. *J. Chem. Phys.* **1985**, *82*, 1156−1166.
(27) Strauss, H. L. *J. Am. Chem. Soc.* **1992**, *114*, 905−907.
(28) Kong, J.; White, C. A.; Krylov, A. I.; Sherrill, D.; Adamson, R. D.; Furlani, T. R.; Lee, M. S.; Lee, A. M.; Gwaltney, S. R.; Adams, T. R.; Ochsenfeld, C.; Gilbert, A. T. B.; Kedziora, G. S.; Rassolov, V. A.; Maurice, D. R.; Nair, N.; Shao, Y. H.; Besley, N. A.; Maslen, P. E.; Dombroski, J. P.; Daschel, H.; Zhang, W. M.; Korambath, P. P.; Baker, J.; Byrd, E. F. C.; Van Voorhis, T.; Oumi, M.; Hirata, S.; Hsu, C. P.; Ishikawa, N.; Florian, J.; Warshel, A.; Johnson, B. G.; Gill, P. M. W.; Head-Gordon, M.; Pople, J. A. *J. Comput. Chem.* **2000**, *21*, 1532−1548.

(29) Frisch, M. J.; Trucks, G. W.; Schlegel, H. B.; Scuseria, G. E.; Robb, M. A.; Cheeseman, J. R.; Zakrzewski, V. G.; Montgomery, J. A., Jr.; Stratmann, R. E.; Burant, J. C.; Dapprich, S.; Millam, J. M.; Daniels, A. D.; Kudin, K. N.; Strain, M. C.; Farkas, O.; Tomasi, J.; Barone, V.; Cossi, M.; Cammi, R.; Mennucci, B.; Pomelli, C.; Adamo, C.; Clifford, S.; Ochterski, J.; Petersson, G. A.; Ayala, P. Y.; Cui, Q.; Morokuma, K.; Malick, D. K.; Rabuck, A. D.; Raghavachari, K.; Foresman, J. B.; Cioslowski, J.; Ortiz, J. V.; Stefanov, B. B.; Liu, G.; Liashenko, A.; Piskorz, P.; Komaromi, I.; Gomperts, R.; Martin, R. L.; Fox, D. J.; Keith, T.; Al-Laham, M. A.; Peng, C. Y.; Nanayakkara, A.; Gonzalez, C.; Challacombe, M.; Gill, P. M. W.; Johnson, B. G.; Chen, W.; Wong, M. W.; Andres, J. L.; Head-Gordon, M.; Replogle, E. S.; Pople, J. A. *Gaussian 98W*, revision A.11.4; Gaussian, Inc.: Pittsburgh, PA, 1998.

(30) Matsuzawa, N.; Seto, J.; Dixon, D. A. *J. Phys. Chem. A* **1997**, *101*, 9391−9398.

(31) Xu, Z.-F.; Xie, Y.; Feng, W.-L.; Schaefer, H. F. *J. Phys. Chem. A* **2003**, *107*, 2716−2729.

(32) Spears, K. G. *J. Phys. Chem. A* **1997**, *101*, 6273−6279.

(33) Jonas, V.; Thiel, W. *Organometallics* **1998**, *17*, 353−360.

(34) Schmidling, D. G. *J. Mol. Struct.* **1975**, *24*, 1−8.